Journal of King Saud University – Science 32 (2020) 1074–1080

Contents lists available at ScienceDirect

Journal of King Saud University – Science

journal homepage: www.sciencedirect.com

Original article

Controlling the structural properties of pure and aluminum doped zinc oxide nanoparticles by annealing

A. Narjis [a,*], H. El Aakib [a], M. Boukendil [b], M. El Hasnaoui [c], L. Nkhaili [a], A. Aberkouks [d], A. Outzourhit [a]

[a] Nanomaterials for Energy and Environment Laboratory, Physics Department, Faculty of Sciences Semlalia, Cadi Ayyad University, PO Box 2390, Marrakech 40000, Morocco
[b] LMFE, Département de Physique, Université Cadi Ayyad, Faculté des Sciences Semlalia, B.P. 2390, Marrakech, Morocco
[c] LASTID Laboratory, Physics Department, Faculty of Sciences, Ibn Tofail University, B.P:133, 14000 Kenitra, Morocco
[d] Laboratoire de chimie de Coordination et de Catalyse, Département de Chimie, Faculté des Sciences Semlalia, Cadi Ayyad University. BP 2390, 40001 Marrakech, Morocco

ARTICLE INFO

Article history:
Received 12 January 2019
Revised 15 April 2019
Accepted 9 October 2019
Available online 24 October 2019

Keywords:
Aluminum doped Zinc oxide
Annealing
Crystallite size
Sol-gel

ABSTRACT

Zinc oxide (ZnO) and aluminum doped zinc oxide (AZO) nanoparticles were synthesized by a typical sol-gel method. The effect of the doping and the annealing temperatures were studied. The dopant percentage of 4% was fixed. XRD patterns showed that ZnO and Al doped ZnO nanoparticles exhibit good crystallization. The crystallite size was shown to decrease by doping and increase by increasing the annealing temperature in the range 350–650 °C. The incorporation of aluminum atoms in the ZnO lattice was confirmed by performing the FTIR spectra. However, the EDX analysis shows that only some aluminum atoms were incorporated.

1. Introduction

Among semiconducting oxides, ZnO is one of the most studied because of its unique physical properties. In fact, it exhibits high carrier mobility, wide band gap (E_g = 3.3 eV), good stability (low reactivity in the ambient air) and non toxicity, to name just a few. These properties prompt it to be used in several technologies such as gas sensors (Galstyan et al., 2015), photocatalysts (Shirdel and Behnajady, 2017), thermal mirrors (Wang, 2004), optoelectronic fields (Wang, 2004) and piezoelectric layers (Yan and Chuan-sheng, 2009). This is why several studies were devoted to study physical properties of undoped and doped ZnO nanoparticles (Kumar et al., 2018; Kumar et al., 2017; Kumar et al., 2017; Straube et al., 2017; Wang, 2015; Krstulović, 2018).

ZnO presents three crystalline structures, namely cubic zinc blend, rocksalt and hexagonal wurtzite. The hexagonal wurtzite-type structure is the most stable at room temperature and under the ambient pressure, with lattice parameters of *a = 0.32495 nm* and *c = 0.52069 nm* (Morkoç and Özgür, 2009).

ZnO is a n-type semiconductor material. Its conductance is due to the stoichiometry deviation caused by the oxygen vacancies and zinc interstices (Janotti and Van de Walle, 2009), so that the exact chemical formula of the resulting compound is ZnO_{1-x} (x is the missing molar percentage to complete the stoichiometry of the ZnO compound). However, this disadvantage can be reduced by doping with selective group III ions such as Ga^{3+}, B^{3+} and Al^{3+} (Claflin et al., 2006; Jood et al., 2011; Lin et al., 2009; Bhosle et al., 2007). In particular, Al^{3+} is a preferred dopant because of the abundance in nature of the used precursors for the synthesis and their low cost. Al doped ZnO nanoparticles were used for highly sensitive CO gas sensors (Hjiri et al., 2014), as catalyst support (Behrens et al., 2013) and in optoelectronic devices (Rotella et al., 2017).

In Al doped ZnO (AZO), Al^{3+} ions substitute Zn^{2+} ions in the lattice. Consequently, the number of electrons increases and this enhances the electrical conductivity (Minami, 2005; Özgür et al., 2005). However, the AZO phase has to be pure to avoid carrier scatterings on the disorder location and therefore ensure good carrier mobility (Goswami et al., 2018). Study of structural properties is

* Corresponding author.
E-mail address: nrjs78@yahoo.fr (A. Narjis).
Peer review under responsibility of King Saud University.

Production and hosting by Elsevier

https://doi.org/10.1016/j.jksus.2019.10.004
1018-3647/

interesting as they affect the other physical properties (Kumar et al., 2018; Kumar et al., 2017; Kumar et al., 2017).

In this paper, pure ZnO and AZO nanoparticles have been synthesized by a typical sol-gel method followed by thermal annealing at 350, 450, 550 and 650 °C. The prepared samples are destined to study the thermoelectric properties of AZO powders. The optimum aluminum molar percentage to have good thermoelectric figure of merit is around 3–4% (Qu et al., 2011; Cheng et al., 2009; Jantrasee et al., 2016). Taking into account the expected small loss of the aluminum content during the synthesis, the starting aluminum percentage was of 4% in the present study. Structural studies showed that the prepared phases are pure with observed shifts in peaks positions indicating the incorporation of the aluminum atoms in the ZnO lattice. The crystallite size was shown to decrease by doping and increase by increasing the annealing temperature.

2. Experimental detail

Aluminum nitrate ($Al(NO_3)_3 9H_2O$) and zinc acetate ($Zn(CH_3COO)_2 2H_2O$) aqueous solutions were used as precursors. The aluminum nitrate and zinc acetate solutions were separately prepared in distilled water as a solvent. The volume of each solution was 100 mL with a concentration of 0.5 M. Then 50 mL of the mixture were prepared while taking into account the aluminum percentage (drops of the aluminum nitrate were added on the zinc acetate solution with magnetic stirring using bar magnets). Then, 50 mL of citric acid (0.5 M) was slowly added as a catalyst and a complex agent. The solution was stirred for 30 min and then heated at 80 °C for 24 h. The obtained powder was washed several times, subsequently by distilled water and acetone over filter paper. Samples were then annealed in a Nabertherm box furnace for 5 h after heating at a rate of 15 °C/min. This duration

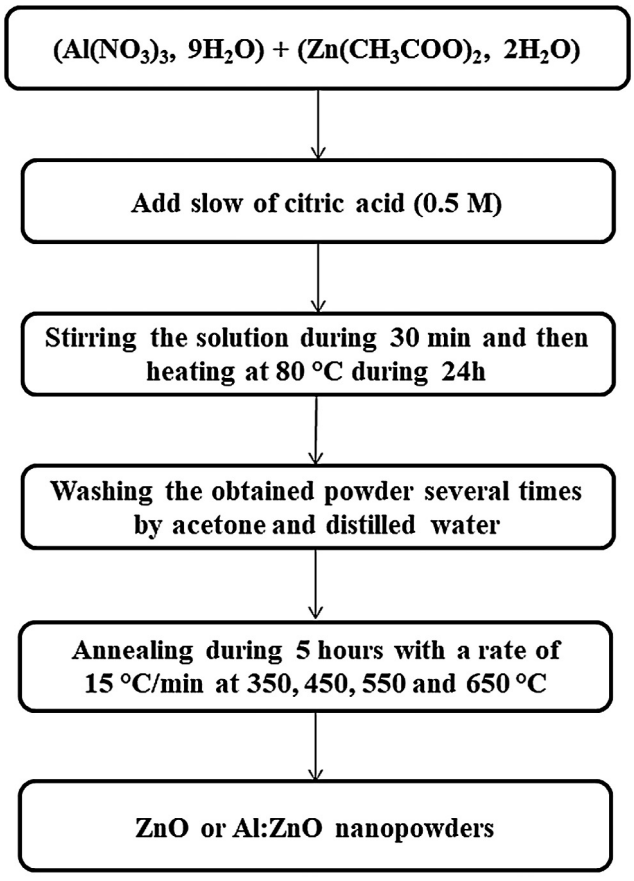

Fig. 1. Schematic of the synthesis of ZnO and AZO nanoparticles.

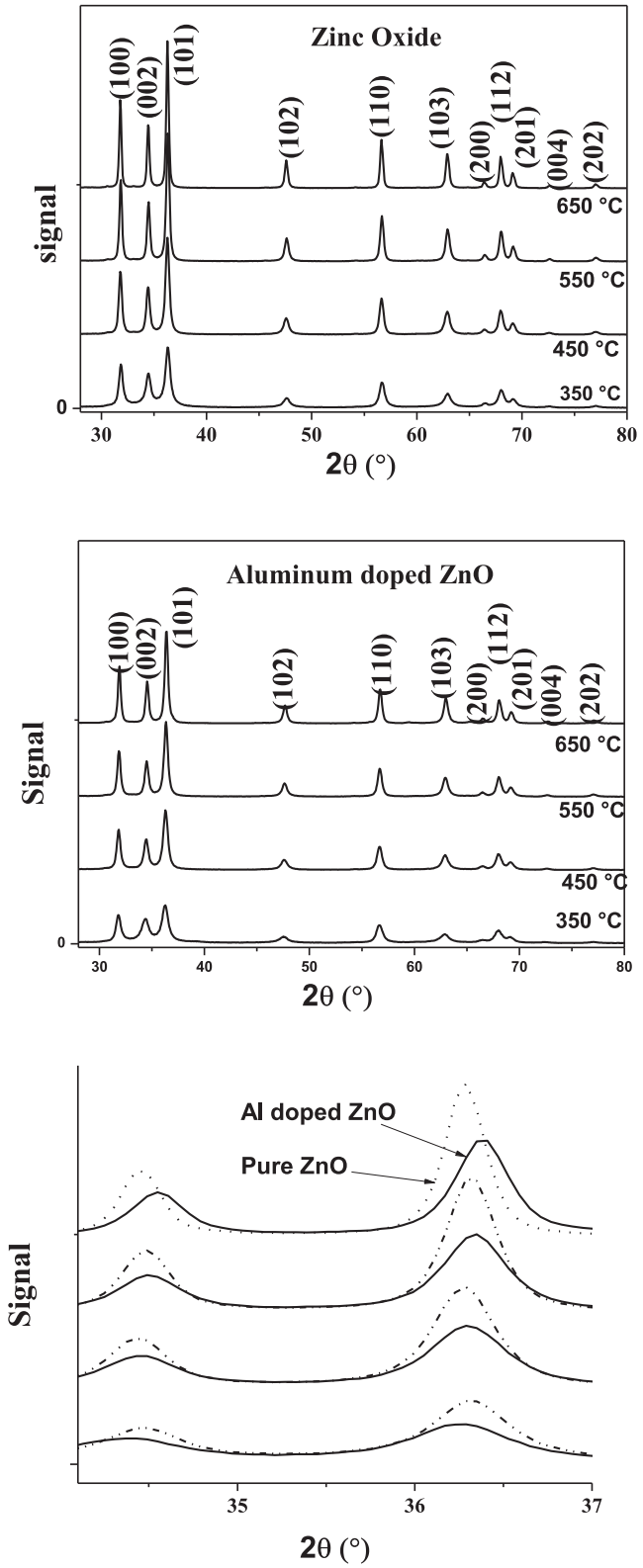

Fig. 2. XRD patterns of the ZnO and AZO nanopowders prepared by the sol-gel method after annealing at various temperatures.

was chosen to be so long to ensure good crystallinity and was dictated from previous works (Aberkouks et al., 2018; Binner et al., 2008). The final annealing temperatures were 350, 450, 550 and 650 °C. The schematic of synthesis route is displayed in Fig. 1. The XRD patterns were taken using an XPERT-3 diffractometer with a copper anticathode. The KBr method was employed to take the FTIR spectra using a Bruker vertex70 DTGS and a Shimadzu UV-PC spectrophotometer, respectively. An amount of 0.001 g of each powder was diluted in 0.099 g of KBr powder. The mixtures were pressed to form circular pellets to realize the FTIR analysis. The Scanning Electron Microscopy (SEM) and the EDX Spectroscopy were performed using a VEGA3 TESCAN.

3. Results and discussion

Fig. 2 shows the XRD patterns of the synthesized ZnO and AZO nanoparticles. According to pure ZnO reference (00-036-1451), all peaks correspond to the hexagonal wurzite structure of ZnO. The obtained phase is pure and no peak was observed to correspond to aluminum, which may indicate that aluminum atoms were successfully incorporated in the ZnO lattice.

Qualitative study of the crystallite size was performed using the Debye-Scherrer equation:

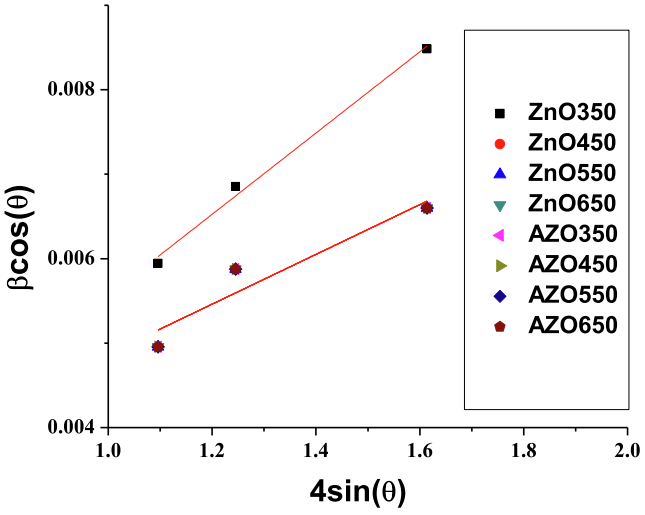

Fig. 3. W-H plots.

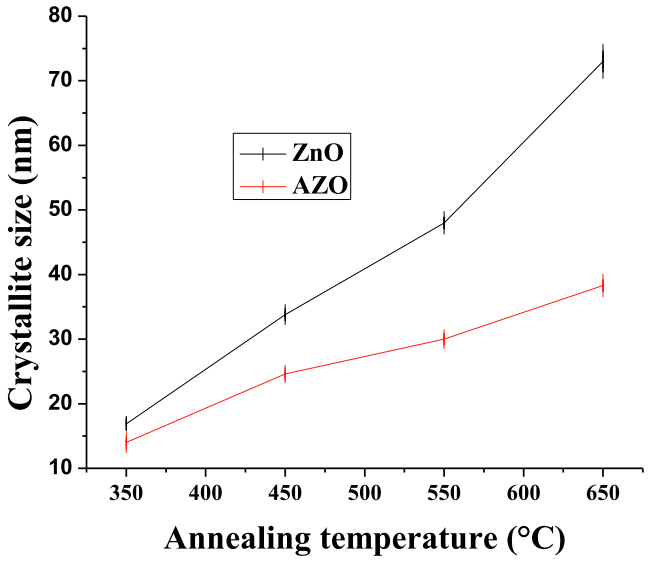

Fig. 4. Crystallite size as function of the annealing temperature for ZnO and AZO nanoparticles.

$$D = \frac{K\lambda}{\beta\cos(\theta)} \quad (1)$$

where $K = 0.9$ is a constant, $\lambda = 1.5406\,Å$ is the wavelength of the used radiation Cu(K_α). β is the Full Width at the Half Maximum and θ is the Bragg diffraction angle.

XRD patterns also offer the possibility to study the strain (ε) in the Williamson-Hall (W-H) analysis. The strain is a measure of the dislocation-induced a given distribution of lattice constants. Assuming that the strain is uniform in all directions, the FWHM is related to the Brag angle as following:

$$\beta\cos(\theta) = \frac{K\lambda}{D} + 4\varepsilon\sin(\theta) \quad (2)$$

The W-H plots are shown in Fig. 3 (only the linear part is considered). The crystallite sizes and strain for each sample summarized in Table 1. The variation of crystallite size with the annealing temperature for pure and doped ZnO is also shown in Fig. 4. The obtained values are comparable to that found by Goswami et al. (2018). It is observed that the crystallite size decreases by doping. This is due to the fact that the ionic Al radius is smaller than the ionic zinc radius and the Al-O covalent bond is shorter than the Zn-O bond. By doping, the sintering slows down

Table 1
Crystallite size, strain and lattice parameters for the synthesized ZnO and AZO samples.

Annealing temperature (°C)	ZnO				AZO			
	Sample	Crystallite size (nm)	Strain	Lattice parameters (Å)	Sample	Crystallite size (nm)	Strain	Lattice parameters (Å)
350	ZnO350	16.6 ± 0.2	0.048	*a = 3.25* *c = 5.21*	AZO350	14.0 ± 0.6	*0.029*	*a = 3.25* *c = 5.22*
450	ZnO450	33.8 ± 0.6	0.029	*a = 3.25* *c = 5.21*	AZO450	24.6 ± 0.4	*0.029*	*a = 3.25* *c = 5.21*
550	ZnO550	48.0 ± 0.8	0.029	*a = 3.25* *c = 5.21*	AZO550	30.0 ± 0.5	*0.029*	*a = 3.25* *c = 5.20*
650	ZnO650	73.0 ± 1.7	0.029	*a = 3.25* *c = 5.21*	AZO650	38.3 ± 0.8	*0.029*	*a = 3.24* *c = 5.20*

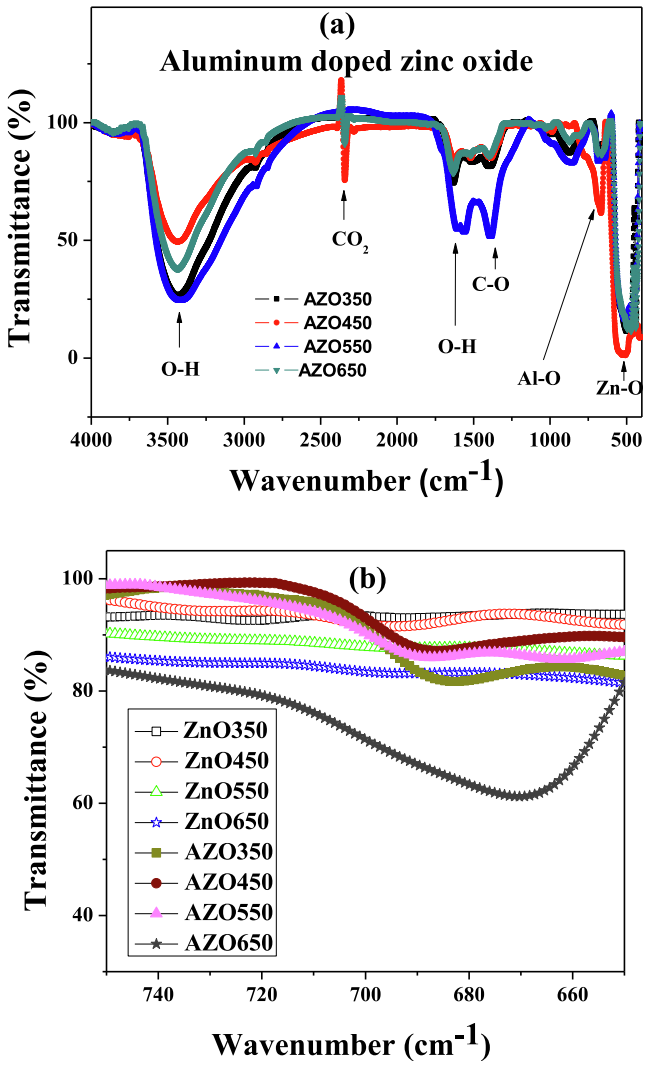

Fig. 5. FTIR spectra of nanoparticles of: (a) AZO and (b) pure ZnO and AZO.

during the sol-gel process (Mazaheri et al., 2008). On the other hand, the crystallite size increases by increasing the annealing temperature. This was previously explained by assuming that small crystallites merge into the larger ones at high temperature (Omri et al., 2014; Mathew et al., 2012; Mhlongo et al., 2014). On the other hand, the strain is observed to be constant, at least for the annealing temperature range 450–650 °C. This is an indication that the observed shifts in XRD peaks are due to the incorporation of aluminum atoms in the ZnO lattice.

The FTIR spectra of the AZO nanoparticles are displayed in Fig. 5-a. Several bonds are shown, including Zn-O, Al-O and O-H. The C-O and O-H bands can be due to the sol-gel process and some organic residues. The absorption band around 2300 cm^{-1} is associated to the atmospheric air. For comparison, the FTIR spectra of the ZnO nanoparticles are shown along with that of the AZO nanoparticles (Fig. 5-b). The Al-O formation confirms the incorporation of the aluminum atoms in the ZnO lattice. It is observed that the annealing at 650 °C results in an intense inflection in the transmission around the Al-O bond frequency, which implies that this annealing is suitable for ensuring the good incorporation of aluminum atoms.

The SEM images of the AZO nanoparticles are displayed in Fig. 6. Also shown are SEM images of the ZnO nanoparticles for the annealing temperatures of 350 and 450 °C. All samples exhibit similar grain shape. Similar to Singh et al. (2016), the distribution of particles size are shown in Fig. 7 We notice that the grains are micro-sized with a size in the order of 2 μm and it is not affected by the annealing or by the doping (shown in Table 2). The obtained grains are bigger than these previously obtained in the literature (Wang, 2015; Jun and Koh, 2013; Kondratiev et al., 2013; Nafees et al., 2013). This may be due to the long annealing duration.

EDS analyses of the so synthesized nanoparticles are shown in Table 2. It is shown that all samples exhibit almost the expected stoichiometry, expect the sample ZnO350. In fact, it is shown that stoichiometry is improved with annealing. However, the aluminum percentage in the AZO nanoparticles did not reach the starting composition (4%) as shown in Fig. 8, indicating that some aluminum atoms do not successfully substitute into the ZnO lattice. This observation was also observed by Akdağ et al. (2016).

Controlling the crystallite size by annealing is an interesting finding as it leads to an easy way of controlling of the importance of the ZnO power in several technologies. In photocatalysts, the power depends upon the ability of the material to generate electrons and holes by light irradiation. This can be achieved by reaching an available energy band gap. The latter depends on the crystallite size (Tyagi and Vedeshwar, 2001; Marotti et al., 2006). Indeed, at the nanoscale, as the crystallite size increases, the number of atoms increases, the number of overlapping of energy levels increases and consequently the gap between the valence band and the conductance band decreases. Improving photocatalytic performance of ZnO nanostructure was achieved by Ye et al. (2006). Furthermore, ZnO is a good candidate for solar cells (Pietruszk et al., 2015; Nkhaili et al., 2015; Vittal and Ho, 2017) and controlling its band gap leads to enhancing its performance in term of electron-holes generation. The crystallite size also influences the gas sensing, which is due to the increase in surface to volume ratio and therefore results in the increasing of the gas molecules at the surface. Enhancement in alcohol vapor sensitivity of Cr doped ZnO gas sensor was observed in reference (Mehdi Hassan et al., 2017). Also, optimizing the crystallite size of polypropylene/zinc oxide nanocomposites was shown to enhance their mechanical, thermal and flow properties (Esthappan et al., 2015).

4. Conclusion

Pure ZnO and Al-doped ZnO nanoparticles were successfully synthesized by the sol-gel method using aluminum nitrate and zinc acetate as precursors. It was shown that the annealing lead to good crystallization. The crystallite size decreased by doping, which is ascribable to the difference between the ionic radii of zinc and aluminum, and increases by increasing the annealing temperature because of the merging of the smaller crystallites into the larger ones. The FTIR spectra revealed the formation of several bonds, including the Zn-O bond in all samples and the Al-O bond in the AZO samples, especially for the annealing at 650 °C. However, The atomic EDS analyses showed that only some aluminum atoms successfully substitute the Zn atoms. This substitution can be improved by a suitable annealing.

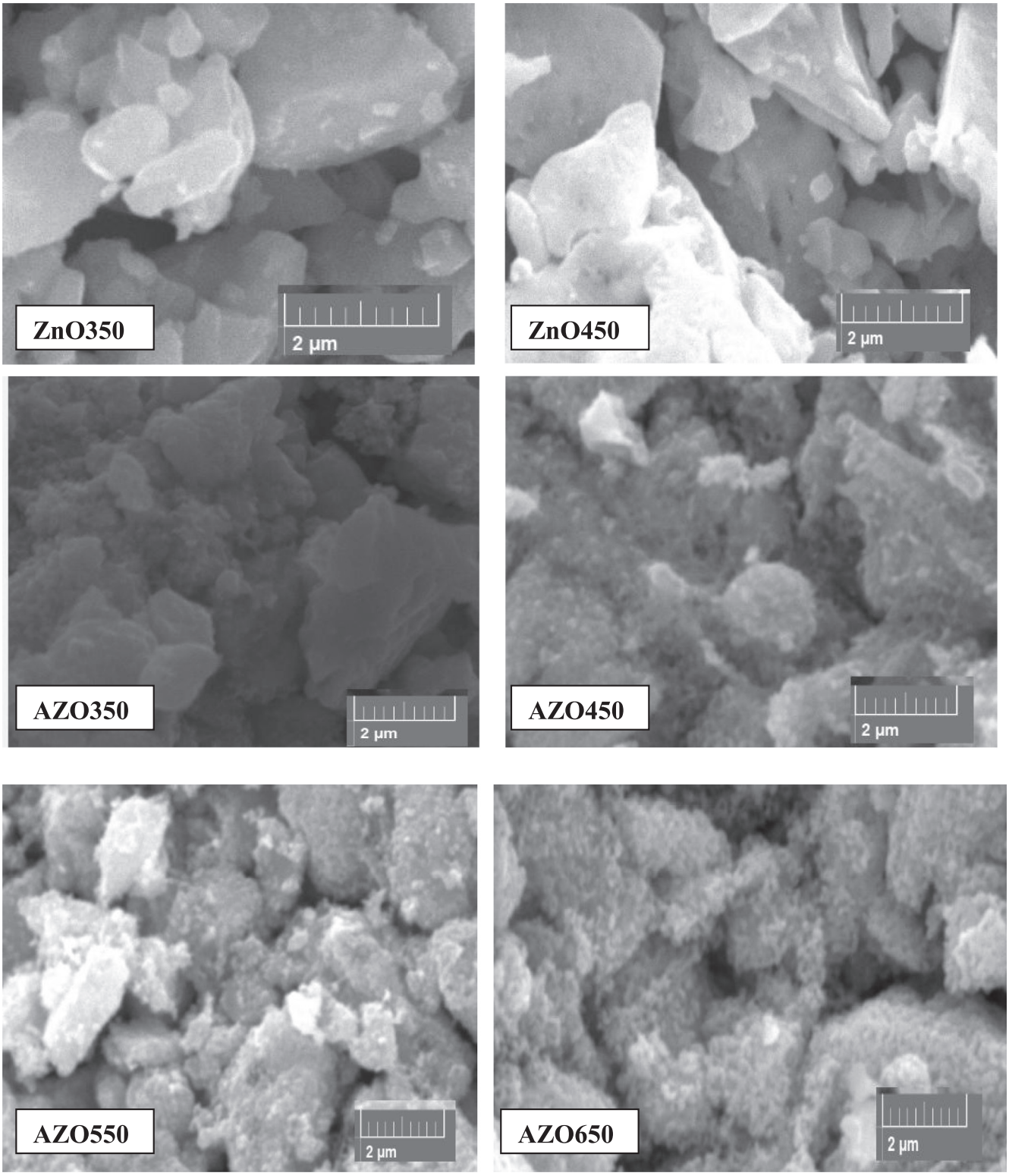

Fig. 6. SEM images for various samples.

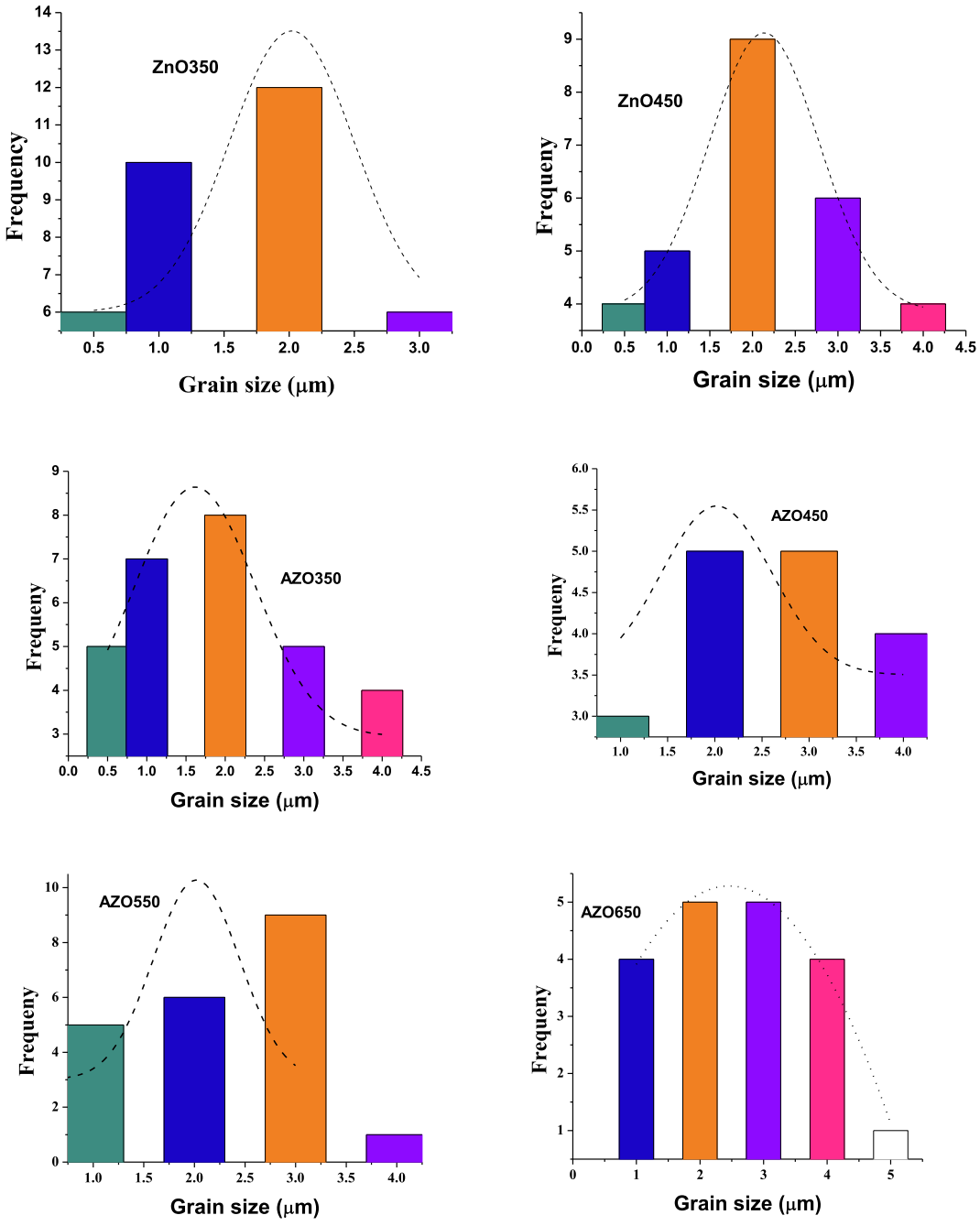

Fig. 7. Gaussian fit to obtain the distribution of the particle size.

Table 2
EDS atomic percentages in the synthesized AZO samples.

Sample	Mean grain size (μm)	Zinc percentage	Oxygen percentage (%)	Aluminum percentage (%)
ZnO350	2	78.71	21.29	–
ZnO450	2.1	56.52	43.48	–
AZO350	2	51.21	45.92	2.86
AZO450	2.1	40.91	56.17	2.92
AZO550	2	32.44	63.97	3.59
AZO650	2.2	47.28	49.92	2.80

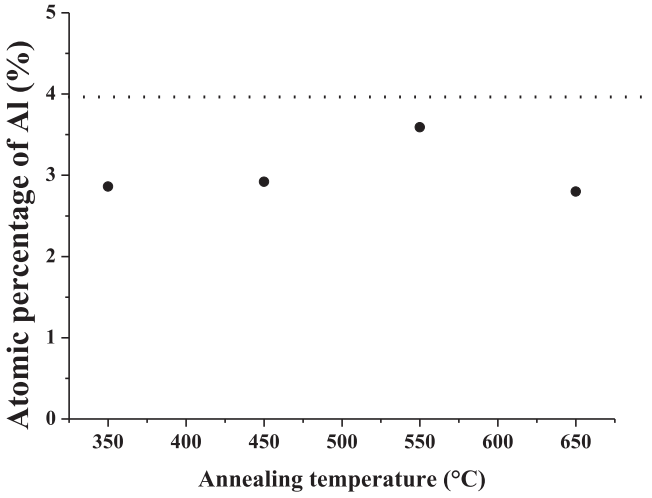

Fig. 8. EDS atomic percentage of aluminum in the AZO samples as a function of annealing temperature.

References

Aberkouks, A., Abdelkader Mekkaoui, A., Boualy, B., El Houssame, S., Ait Ali, M., El Firdoussi, L., 2018. Selective oxidation of styrene to benzaldehyde by Co-Ag codoped ZnO catalyst and H2O2 as oxidant. Adv. Mater. Sci. Eng., 7 Article ID 2716435.

Akdağ, A., Budak, H.F., Yılmaz, M., Efe, A., Büyükaydın, M., Can, M., Turgut, G., Sönmez, E., 2016. Structural and morphological properties of Al doped ZnO nanoparticles. J. Phys. Conf. Series 707, 12020.

Behrens, M., Lolli, G., Muratova, N., Kasatkin, I., Havecker, M., d' Alnoncourt, M., Schlögl, R.N., Muhler, M., Schlogl, R., 2013. The effect of Al-doping on ZnO nanoparticles applied as catalyst support. PCCP 15 (5), 1374–1381.

Bhosle, V., Prater, J.T., Yang, F., Burk, D., Forrest, S.R., Narayan, J., 2007. Gallium-doped zinc oxide films as transparent electrodes for organic solar cell applications. J. Appl. Phys. 102 (2), 1–5.

Binner, J., Vaidhyanathan, B., Wang, J., Price, D., Reading, M., 2008. Evidence for non-thermal microwave effects using single and multimode hybrid conventional/microwave systems. J. Microw. Power Electromagn. Energy. 42 (2), 47–63.

Cheng, H., Xu, X.J., Hng, H.H., Ma, J., 2009. Characterization of Al-doped ZnO thermoelectric materials prepared by RF plasma powder processing and hot press sintering. Ceram. Int. 35, 3067–3072.

Claflin, B., Look, D.C., Park, S.J., Cantwell, G., 2006. Persistent n-type photoconductivity in p-type ZnO. J. Cryst. Growth 287 (1), 16–22.

Esthappan, S.K., Ajalesh, B., Nair, A.B., Rani Joseph, R., 2015. Effect of crystallite size of zinc oxide on the mechanical, thermal and flow properties of polypropylene/zinc oxide nanocomposites. Composite B 67, 145–153.

Galstyan, V., Comini, E., Baratto, C., Faglia, G., Sberveglieri, G., 2015. Nanostructured ZnO chemical gas sensors. Ceram. Int. 41 (10), 14239–14244.

Goswami, M., Adhikary, N.C., Bhattacharjee, S., 2018. Effect of annealing temperatures on the structural and optical properties of zinc oxide nanoparticles prepared by chemical precipitation method. Optik 158, 1006–1015.

Hjiri, M., El Mir, L., Leonardi, S.G., Pistone, A., Mavilia, L., Neri, G., 2014. Al-doped ZnO for highly sensitive CO gas sensors. Sens. Actuators, B 196, 413–420.

Janotti, A., Van de Walle, C.G., 2009. Fundamentals of zinc oxide as a semiconductor. IOPscience Rep. Prog. Phys. 72, 126501–126529.

Jantrasee, S., Moontragoon, P., Pinitsoontorn, S., 2016. Thermoelectric properties of Al-doped ZnO: experiment and simulation. J. Semicond. 37, (9) 092002.

Jood, P., Mehta, R.J., Zhang, Y., Peleckis, G., Wang, X., Siegel, R., Borca-Tasciuc, T., Dou, S., Ramanath, G., 2011. Al-doped zinc oxide nanocomposites with enhanced thermoelectric properties. Nano Lett. 11 (10), 4337–4342.

Jun, M.-C., Koh, J.-H., 2013. Effects of annealing temperature on properties of Al-doped ZnO thin films prepared by sol-gel dip-coating. J. Electr. Eng. Technol. 8 (1), 163–167.

Kondratiev, V.I., Kink, I., Romanov, A.E., 2013. Low temperature Sol-Gel technique for processing Al-doped zinc oxide films. Mater. Phys. Mech. 17, 38–46.

Krstulović, N. et al., May 2018. Parameters optimization for synthesis of Al-doped ZnO nanoparticles by laser ablation in water. Appl. Surf. Sci. 440, 916–925.

Kumar, V., Prakash, J., Pal Singh, J., Hwa Chae, K., Swart, C., Ntwaeaborwa, O.M., Swart, H.C., Dutta, V., 2017. Role of silver doping on the defects related photoluminescence and antibacterial behaviour of zinc oxide nanoparticles. Colloids Surf. B: Biointerfaces 159, 191–199.

Kumar, M., Singh, J.P., Chae, K.H., Kim, J.H., Lee, H.H., Aug. 2018. Structure, optical and electronic structure studies of Ti:ZnO thin films. J. Alloy. Compd. 759, 8–13.

Kumar, H., Singh, J.P., Srivastava, R.C., Patel, K.R., Chae, K.H., Sep. 2017. Synthesis and characterization of DyxCoFe2−xO4 nanoparticles. Superlattices Microstruct. 109, 296–306.

Lin, J.M., Zhang, Y.Z., Ye, Z.Z., Gu, X.Q., Pan, X.H., Yang, Y.F., Lu, J.G., He, H.P., Zhao, B. H., 2009. Nb-doped ZnO transparent conducting films fabricated by pulsed laser deposition. Appl. Surf. Sci. 255 (13–14), 6460–6463.

Marotti, R.E., Giorgi, P., Machado, G., Dalchiel, E.A., 2006. Crystallite size dependence of band gap energy for electrodeposited ZnO grown at different temperatures. Sol. Energy Mater. Sol. Cells 90(15, 2356–2361.

Mathew, J.P., Varghese, G., Mathew, J., 2012. Effect of post-thermal annealing on the structural and optical properties of ZnO thin films prepared from a polymer precursor. Chin. Phys. B 21 (7), 78104.

Mazaheri, M., Zahedi, A.M., Sadrnezhaad, S.K., 2008. Two-step sintering of nanocrystalline ZnO compacts: effect of temperature on densification and grain growth. J. Am. Ceram. Soc. 91 (1), 56–63.

Mehdi Hassan, M., Khan, W., Mishra, P., Islam, S., Naqvi, A.H., 2017. Enhancement in alcohol vapor sensitivity of Cr doped ZnO gas sensor. Mater. Res. Bull. 93, 391–400.

Mhlongo, G.H., Motaung, D.E., Nkosi, S.S., Swart, H.C., Malgas, G.F., Hillie, K.T., Mwakikunga, B.W., 2014. Temperature-dependence on the structural, optical, and paramagnetic properties of ZnO nanostructures. Appl. Surf. Sci. 293, 62–70.

Minami, T., 2005. Transparent conducting oxide semiconductors for transparent electrodes. Semicond. Sci. Technol. 20 (4), S35–S44.

Morkoç, H., Özgür, Ü., 2009. Zinc oxide: fundamentals. Materials and Device Technology. Wiley-VCH Verlag GmbH & Co. KGaA, Weinheim. Chapter 1.

Nafees, M., Liaqut, W., Ali, S., Shafique, M.A., 2013. Synthesis of ZnO/Al:ZnO nanomaterial: structural and band gap variation in ZnO nanomaterial by Al doping. Appl. Nanosc. 3 (1), 49–55.

Nkhaili, L., Elyaagoubi, M., Elmansouri, A., El Kissani, A., El Khalfi, A., Elfathi, A., Ait Ali, M., Outzourhit, A., 2015. Structural, optical and electrical characteristics of zinc oxide and copper oxide films and their heterojunctions. Spectrosc. Lett. 48 (7), 536–541.

Omri, K., Najeh, I., Dhahri, R., EL Ghoul, J., El Mir, L., 2014. Effects of temperature on the optical and electrical properties of ZnO nanoparticles synthesized by sol-gel method. Microelectron. Eng. 128, 53–58.

Özgür, Ü., Alivov, Y.I., Liu, C., Teke, A., Reshchikov, M.A., Dogan, S., Avrutain, V., Cho, S.-J., Morkoç, H.A., 2005. Comprehensive review of ZnO materials and devices. J. Appl. Phys. 98 (4), 1–103.

Pietruszk, R., Witkowski, B.S., Gieraltowsk, S., Caban, P., Wachnicki, L., Zielony, E., Gwozdz, K., Bieganski, P., Placzek-Popko, E., Godlewski, M., 2015. New efficient solar cell structures based on zinc oxide nanorods. Sol. Energy Mater. Sol. Cells. 143, 99–104.

Qu, X., Wang, W., Lv, S., Jia, D., 2011. Thermoelectric properties and electronic structure of Al-doped ZnO. Solid State Commun. 151, 332–336.

Rotella, H., Mazel, Y., Brochen, S., Valla, A., Pautrat, A., Licitra, C., Rochat, N., Sabbione, C., Rodriguez, G., Nolot, E., 2017. Role of vacancy defects in Al doped ZnO thin films for optoelectronic devices. J. Phys. D Appl. Phys. 50 (48), 485106.

Shirdel, B., Behnajady, M.A., 2017. Sol-gel synthesis of Ba-doped ZnO nanoparticles with enhanced photocatalytic activity in degrading rhodamine B under UV-A irradiation. Optik 147, 143–150.

Singh, J.P., Kim, S.H., Won, S.O., Lim, W.C., Lee, I.-J., Chae, K.H., Apr. 2016. Covalency, hybridization and valence state effects in nano- and micro-sized ZnFe2O4. CrystEngComm 18 (15), 2701–2711.

Straube, T., Linders, J., Mayer-Gall, T., Textor, T., Mayer, C., Gutmann, J.S., Jan. 2017. Polyol synthesized aluminum doped zinc oxide nanoparticles - influence of the hydration ratio on crystal growth, dopant incorporation and electrical properties. Mater. Today. Proc. 4, S253–S262.

Tyagi, P., Vedeshwar, A.G., 2001. Grain size dependent optical band gap of CdI2 films. Bull. Mater. Sci. 24 (3), 297–300.

Vittal, R., Ho, K.-C., 2017. Zinc oxide based dye-sensitized solar cells: A review. Renew. Sust. Energ. Rev. 70, 920–935.

Wang, Z.L., 2004. Zinc oxide nanostructures: growth, properties and applications. J. Phys.: Condens. Matter 16, R829–R858.

Wang, A. et al., 2015. Effects of doping and annealing on properties of ZnO films grown by atomic layer deposition. Nanoscale Res. Lett. 10 (1), 75.

Yan, L., Chuan-sheng, L., 2009. Hydro/solvo-thermal syntesis of ZnO crystallite with particular morphology. Sci. Press. Trans. Nanoferrous Metals Soc. China 19, 399–403.

Ye, C., Bando, Y., Shen, G., Golberg, D., 2006. Thickness-dependent photocatalytic performance of ZnO nanoplatelets. J. Phys. Chem. B 110, 15146–15151.